ACS APPLIED MATERIALS & INTERFACES

www.acsami.org

Research Article

Strengthening in Metal/Graphene Composites: Capturing the Transition from Interface to Precipitate Hardening

Fei Shuang, Zhaohe Dai, and Katerina E. Aifantis*

Cite This: https://doi.org/10.1021/acsami.1c05129

Read Online

ACCESS | Metrics & More | Article Recommendations | Supporting Information

ABSTRACT: A promising materials engineering method for improving the strength of crystalline materials is to add obstacles to dislocation motion that induce interface hardening (IH) or precipitate hardening (PH). In this study, molecular dynamics simulations are performed for Ni/graphene composites, revealing for the first time that graphene can strengthen the Ni matrix not only strictly via IH or PH but also through a continuous transition between the two. When graphene behaves like an interface, dislocation pileups form, whereas when it behaves as a precipitate, complex Orowan looping occurs by dislocation cross-slip. IH transitions to PH when the integrity of the graphene-dislocation configuration (GDC) deteriorates, leading to a reduced strengthening effect. Furthermore, the deformation of graphene is found to be an effective signature to indicate the real-time strengthening. This observation relates the graphene strengthening effect on metals to a combination of parameters, such as the GDC integrity, graphene deformation, and dislocation evolution, opening an avenue to tune the mechanical properties by controlling the dislocation movements and manipulating the dislocation−obstacle interaction mechanisms.

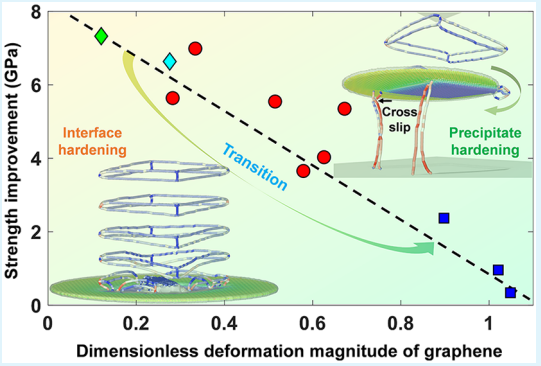

KEYWORDS: *graphene, interface, precipitate, strengthening transition, molecular dynamics*

1. INTRODUCTION

The critical factor that affects the mechanical behavior of crystalline materials is the interaction between dislocations and obstacles.[1,2] In particular, interfaces and precipitates are two classical obstacles, which have been widely used to improve the strength and ductility of crystalline materials through manipulating their size and/or distribution. A critical issue that nanostructured engineering can aid in is the ability to increase the strength of materials without losing their ductility[3−5] since at the nanoscale, internal surfaces could serve as obstacles to block dislocation motion but also act as sinks to absorb dislocations. For nanomaterials, interface hardening (IH) or precipitate hardening (PH) refers to the improvement in strength through the introduction of either interfaces or precipitates.

The ability of interfaces to block dislocation propagation affects the material strength,[6,7] while the absorption of dislocations often alleviates stress concentrations and hence leads to significant improvement in the material ductility.[5] The most commonly observed IH is grain boundary (GB) strengthening. Specifically, nanograined materials,[8,9] nanotwinned materials,[10,11] gradient nanograined materials,[3] and gradient nanotwinned materials[4] have been developed to increase not only the mechanical properties such as strength and ductility but also the thermal stability and conductivity. Twin boundaries are a special class of GBs possessing a low formation energy, and they have been shown to improve the strength not only in metals but also in cubic boron nitride[12] and diamond.[13] Other interfaces such as crystalline/amorphous interfaces,[5] bimetal interfaces,[14] and metal/graphene (Gr) interfaces[15] have been used to block dislocation propagation in nanolaminated materials and bioinspired materials, achieving the simultaneous enhancement of both the yield strength and ductility.

PH has been widely employed in alloy systems such as Ni-based alloys, steels,[16,17] and multiple-element alloys[18−20] to achieve ultrahigh strength and large ductility. It was rationalized in a recent molecular dynamics (MD) study that nanoscale precipitates can simultaneously serve as dislocation sources and obstacles[21] to produce sustained deformability. High-density nanoprecipitation with a minimal lattice misfit was believed to be a key factor for the observed enhancement in strength and ductility.[17]

Although IH and PH have been well understood by extensive experiments and atomistic simulations in the past

Received: March 18, 2021
Accepted: May 6, 2021

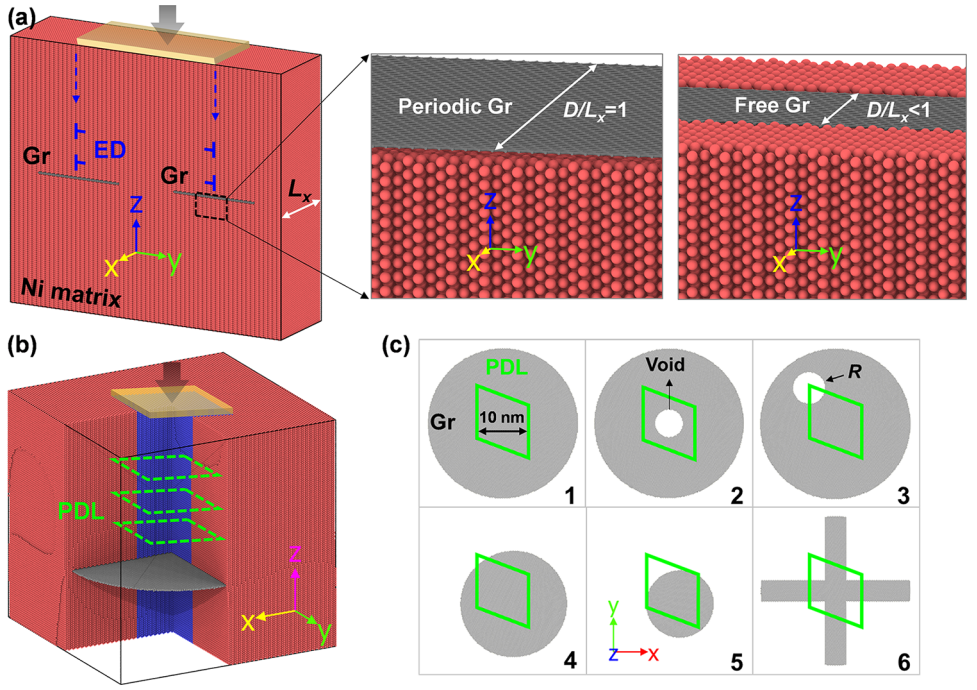

Figure 1. Simulation configurations. (a) Quasi-3D nanoindentation configuration used to produce ED pileups and different Gr nanosheets. (b) Full 3D nanoindentation configuration used to produce a PDL pileup. (c) Six different Gr nanosheets used in (b).

few decades, the differences and connections between them are rarely discussed. In particular, the ad hoc understanding has elucidated specific features of dislocation−obstacle interactions associated with both of these mechanisms. Even though the main difference between interfaces and precipitates is the geometry of their resulting internal surface, what is lacking is insight into the transition between IH and PH as the structure of these obstacles evolves throughout their interaction with dislocations during continuous deformation. Recently, Gr has been used to block dislocation motion in metal matrices, allowing for significant improvement in the strength.[15,22,23] Although numerous MD studies have been dedicated on examining dislocation−Gr interactions in metal/Gr composites, the resulting strengthening effect and deformation mechanisms vary when different loading manners and boundary conditions are used.[24−31] The effect of the Gr structure/morphology on the strengthening mechanism remains unclear. Since the structure/morphology of Gr can be modified as needed, herein we consider Gr as a specific obstacle to study its performance as either a precipitate or an interface in strengthening the Ni matrix by performing MD simulations.

To this end, two novel configurations are set up, which allow either edge dislocations (EDs) or prismatic dislocation loops (PDLs) to form pileups in the same slip plane and interact with Gr directly. These novel MD methods can be used to study the interactions between dislocation pileups and obstacles such as GBs, precipitates, and other interfaces in MD simulations. We show that a key aspect which can control the strengthening mechanisms is the location of the dislocation with respect to Gr. Specifically, we propose a new "parameter" which we call integrity of the graphene-dislocation configuration (GDC); the highest integrity corresponds to when the dislocation is located fully within the Gr, while the integrity is reduced when only part of the dislocation is within the Gr. The integrity of the GDC is also affected by the presence of void-like defects within the Gr. By changing the GDC, it is found that the Gr acts as either an interface or a precipitate or continuously transitions between the two, throughout deformation, to strengthen the Ni matrix. The dislocation propagation mechanisms of IH and PH and the transition from one to another are analyzed by tracking dislocation evolution and Gr deformation. Our findings reveal a complex, coupled effect of the GDC integrity, Gr deformation, and dislocation evolution and emphasize the significance of using large-sized and defect-free Gr in strengthening the metal matrix.

2. METHODS

The LAMMPS software[32] was employed to perform MD simulations for two carefully selected Ni/Gr systems as shown in Figure 1, allowing either simple EDs and PDLs to pile up in front of Gr in face-centred cubic (FCC) Ni matrices. The atomistic model in Figure 1a is a quasi-3D configuration which was used to study ED pileup interactions with Gr. The simulation box had the dimensions of $L_x \times L_y \times L_z$ = 10.3 × 37.8 × 33.8 nm^3, containing ∼1.2 million Ni atoms. The crystallographic directions were x-[$\bar{1}$12], y-[111] and z-[$\bar{1}$10]. Periodic boundary conditions were used in the x- and y-directions and free boundary conditions were used in the z-direction. Two identical Gr nanosheets were placed in the middle of the Ni matrix. Two different types of Grs were considered with the same length (11.0 nm) in the y-direction but a different length D in the x-direction. In the first case, D/L_x = 1, indicating that the Gr is periodic and infinitely long in the x-direction; in the second case, D/L_x < 1, indicating that the Gr is finite. Five finite Grs with different D/L_x were considered. To produce ED pileups at the center of Gr nanosheets, a flat indenter was used with a rectangular shape and dimensions of 19.0 nm to compress portion of the composites with a velocity of 5 m/s in an isothermal-isobaric (NPT) ensemble.

PDL pileups were generated using the model in Figure 1b, which is a full 3D configuration. The simulation box had the dimensions of $L_x \times L_y \times L_z$ = 30.5 × 29.3 × 29.8 nm^3, containing ∼2.4 million Ni atoms. The crystallographic directions were x-[$\bar{1}$10], y-[00$\bar{1}$] and z-[110]. Periodic boundary conditions were used in the x- and y-directions and free boundary conditions were adopted in the z-

https://doi.org/10.1021/acsami.1c05129
ACS Appl. Mater. Interfaces XXXX, XXX, XXX−XXX

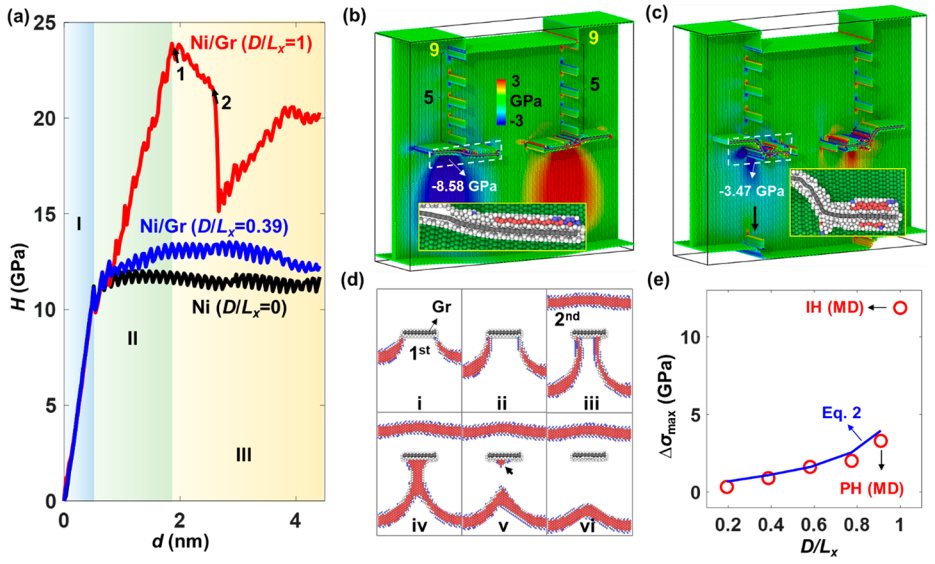

Figure 2. Simulation results of quasi-3D Ni and Ni/Gr samples with EDs. (a) Hardness−depth (H−d) curves for Ni/Gr (D/L_x = 1), Ni/Gr (D/L_x = 0.39), and pure Ni (D/L_x = 0). (b,c) Nucleated dislocations and deformed Gr at points 1 and 2 in (a), respectively. All Ni atoms are colored by the atomic shear stress τ_{yz}, and the gray atoms indicate Gr. (d) Complete dislocation looping process for Ni/Gr (D/L_x = 0.39). (e) Strength improvement of Ni/Gr composites with different D/L_x compared to the pure Ni sample.

direction. To mimic the Gr nanosheets with various morphologies and possible void-like defects that are present in real systems, six types of Grs with different GDC integrities (named as Gr-1, ..., Gr-6) were considered, as shown in Figure 1c. To produce a PDL pileup at the center of Gr nanosheets, a flat indenter with a rhombus shape and dimensions of 10.0 nm compressed portion of the composites with a velocity of 5 m/s in an *NPT* ensemble.

Prior to indentation, all samples were relaxed by energy minimization and then with dynamics relaxation over 10 ps in an *NPT* ensemble. Though the high strain rate is inevitable in conventional MDs due to the intrinsic time scale of atomic vibrations,[33] our previous studies have shown that MDs can provide an insightful understanding of basic dislocation−Gr interaction mechanisms in Cu/Gr and Fe/Gr composites.[25,34] To avoid thermal effects, the temperature was set as 0.1 K in all cases. An additional simulation at 300 K in Figure S1 of the Supporting Information shows the same dislocation−Gr interaction mechanisms as the simulation at 0.1 K, indicating that our findings are valid when thermal effects are considered. For the purpose of comparison, the corresponding pure Ni samples were simulated with the same configuration and loading conditions (at 0.1 K) for both Gr cases considered. The Ni atoms near Gr within a distance of 1.5 Å were removed to avoid atom overlapping. In the experiments, Ni atoms cannot be removed but are deformed near the Gr nanosheets, leading to a larger geometrical mismatch than that in our simulations. This geometrical mismatch can make Gr nanosheets act as dislocation sources. The mismatch, however, will be reduced after dislocation emission and then our simulations will be similar to experiments. Therefore, we believe our MD models are meaningful and are able to capture the basic dislocation−Gr interaction mechanisms.

To avoid the translation in the z-direction, during simulations, all samples were restrained by requiring that the load F imposed by the indenter be countered by an opposite body force—F/N distributed equally among the bottom atoms, where N is the number of bottom atoms with a thickness of 2.0 nm (Figure 1a) or 1.5 nm (Figure 1b). Ideally, dislocations should move far away from graphene after transmission or bypass it due to the very small lattice friction of Ni, and these dislocations will not affect new dislocation−Gr interactions. Therefore, the usage of the free bottom conditions can better mimic the real dislocation−graphene interactions. Otherwise, a very large dimension is needed in the z-direction, which is unwise for MD simulations. We also show in Figure S2 that the periodic and free lateral boundaries have no effect on simulating dislocation−Gr interaction mechanisms, indicating that the findings in our study are convergent with supercell dimensions.

The interaction between Ni atoms was described by the embedded-atom method potential[35] and the C−C interaction in the Gr was modeled by the Stillinger−Weber (SW) potential. Both the elastic deformation and fracture of Gr can be well captured by this potential.[36] The Ni−C interaction was described by the Lennard-Jones potential with parameters of 0.023049 eV and 2.852 Å, which has been confirmed by density functional theory calculations[15] and has been successfully applied in MD simulations for nano-indentation[37] and bending[27] of Ni/Gr composites. All simulation results were visualized by the OVITO software.[38] Common Neighbor Analysis (CNA) was used to identify defect atoms and the atomic von Mises strain was used to track inelastic deformation.[39] The Dislocation Extraction Algorithm was used to extract and depict discrete dislocation lines.[40]

3. RESULTS AND DISCUSSION

3.1. ED Pileup−Gr Interactions. We first demonstrate the two strengthening mechanisms (IH and PH) by simulating ED pileup−Gr interactions in the unique nanoindentation configuration shown in Figure 1a. We use the hardness−depth (H−d) curves in Figure 2a to show that the Gr width significantly affects the strengthening effect. Based on the H−d curve of Ni/Gr (D/L_x = 1), one can recognize three deformation stages. In stage I, all samples deform elastically with the same slope, indicating that the Gr inclusions have no influence on the elastic response of the Ni matrix. In stages II and III, however, Ni/Gr (D/L_x = 1) exhibits a significantly higher strengthening effect than that of the other cases, including pure Ni and Ni/Gr (D/L_x = 0.39). In the pure Ni case, the plateau in stages II and III is caused by the stable plastic flow by which two ED pairs nucleate and escape from the free bottom. The resulting strengthening effect is negligible because there is no obstacle in the sample to block dislocation motion.[34] Our results show that the insertion of Gr sheets alters the dislocation propagation and strengthening effect but in different ways, depending on the width of the Gr sheets. Such differences are more pronounced at the end of stage II

https://doi.org/10.1021/acsami.1c05129
ACS Appl. Mater. Interfaces XXXX, XXX, XXX−XXX

and imply completely different strengthening mechanisms, which we discuss via the detailed ED−Gr interaction process.

To elucidate the deformation mechanism of Ni/Gr (D/L_x = 1), we present in Figure 2b,c the deformation state in the Ni/Gr systems at points 1 and 2 labeled in Figure 2a. It is seen that the continuous increase in hardness of Ni/Gr (D/L_x = 1) in stage II (until point 1) results from the increasing back stress when more EDs form pileups. Particularly, at point 1, nine EDs nucleate from the top surface, the first four of which are absorbed by the Ni/Gr interface, resulting in a significant phase transition near the Ni/Gr interface as indicated in the inset of Figure 2b, while the subsequent five EDs form a pileup. In stage II, the periodic Gr (D/L_x = 1) acts as a strong barrier to block dislocation propagation. Note that dislocation absorption does not change the slope of the curve in stage II, but once transmission begins in stage III, the slope becomes negative (Figure 2a), suggesting that direct dislocation transmission corresponds to Gr yielding as an interface. In stage III, dislocations transmit across Gr and then leave from the bottom (Figure 2c), leading to the decrease of hardness at point 2 in Figure 2a. This is further supported by the highly accumulated atomic shear stress under the Gr in Figure 2b,c (decreased from 8.58 to 3.47 GPa after transmission) and is in good agreement with our previous Cu/Gr MD simulations.[34] The phase transitionfrom FCC to hexagonal close-packed (HCP) near the metal/Gr interfaces in the inset of Figure 2c also indicates the severe dislocation−Gr interactions. Therefore, when D/L_x = 1, the inserted Gr has the highest GDC integrity since it is infinitely large along the dislocation line direction due to periodic boundary conditions, resulting in IH.

The dislocation absorption in Figure 2b results from the spreading of the dislocation core, which is quantitatively presented in Figure S3. The continuous absorption and core spreading further result in the phase transition from FCC into HCP in Figure 2b,c. Previous MD studies have shown that dislocation absorption and core spreading play a crucial role in optimizing the strength and the ductility of the Cu−Nb multilayers.[14] Our simulations indicate that metal/Gr interfaces also contribute to improving ductility by core spreading and phase transitions. On the other hand, our recent MD simulations showed that only two dislocations were blocked by Gr sheets in Cu/Gr composites, and the obtained strength improvement in Cu/Gr was smaller than in Ni/Gr.[34] The discrepancy between them can be attributed to the different shear strengths of the metal/Gr interface because interface sliding is necessary to accommodate the deformation due to dislocation transmission.[15]

Figure 2d presents the side-view of a complete ED−Gr interaction process for Ni/Gr (D/L_x = 0.39) at different deformation states, and Figure S4 gives the corresponding deflection magnitude for the deformed Gr. It is seen that once the first dislocation approaches the Gr at state i, the middle segment of the dislocation is completely absorbed by the Ni/Gr interface, while the rest of the dislocation segments bow out as the two ends are pinned at the Gr's edges. The bow-out dislocation segments further move downward at state ii. As the second dislocation approaches Gr, the bow-out dislocation segments glide along the bottom surface of Gr at state iii, connect at state iv, detach from Gr at state v, and move downward at state vi. The residual stacking fault segments at state iv indicated by the arrow in Figure 2d completely disappear at state vi. The evolution of Gr deflection in Figure S3 demonstrates that Gr is significantly sheared at state i even before the occurrence of the dislocation bow-out and looping process. Most of the Gr deformation occurs before state iii and Gr undergoes less deformation during the bypassing process. After the first dislocation bypass, Gr is sheared with out-of-plane deflection of around 3.0 Å to accommodate the dislocation propagation. Since no dislocations are completely blocked and all dislocations bypass Gr by bowing out and looping, the free Gr (D/L_x < 1) with reduced GDC integrity gives rise to PH. Note that we observe significant Ni/Gr interface sliding after dislocations bypass graphene (Figure S4), indicating that the interface shear strength also affects the strengthening effect of Gr as a precipitate.

Previous works have shown two main PH mechanisms, that is, the cutting mechanism and the Orowan looping (or bowing) mechanism, depending on the precipitate size. For small precipitates, the cutting mechanism dominates; otherwise, the looping mechanism dominates.[41] In the present simulations, although Gr is significantly sheared after the dislocation bypasses it (see Figure S4), the observed PH is dominated by the Orowan looping mechanism as evidenced by the bowed out dislocation and residual dislocation at the bottom of Gr (Figure 2d). Shearing Gr directly requires a significantly higher stress (Figure 2b), which is not possible for the interaction of dislocations with free Gr. The residual Orowan loop that sometimes is observed for precipitates is not seen here because the Ni/Gr interface absorbs it as seen in free Gr (Figure 2d).

ED pileup−Gr interaction simulations in Figure 2 have revealed two different strengthening mechanisms in metal/Gr composites: IH and PH. It is worth noting that in general, IH works much better than PH in terms of strengthening. Based on the dislocation−Gr interaction, we can see a transition from IH to PH as D/L_x approaches unity. We further illustrate the strength improvement of Ni/Gr composites and the mechanism transition by calculating the maximum difference of hardness between Ni/Gr and Ni in stage II and plotting it in Figure 2e with respect to the width ratio D/L_x. In this plot, it is seen as D/L_x = 1, the strength increases drastically, indicating this transition from IH to PH. The strengthening effect of IH may then be described by the dislocation pileup model or the known Hall−Petch relationship[42,43]

$$\Delta\sigma_{IH} = k_{Gr} d^{-0.5} \tag{1}$$

where k_{Gr} is the Hall−Petch constant slope measuring the ability of Gr to block dislocation motion, and d denotes grain size. Letting $d = L_z/2$ = 16.9 nm, we have k_{Gr} = 1.54 MPa$\sqrt{m}$, which is much higher than k_{TB} = 0.70 MPa$\sqrt{m}$ for nanotwinned Ni.[44] This indicates that Gr may better block dislocation propagation than GBs as long as D/L_x = 1 in a Ni matrix. This conclusion cannot be generalized for all metal/Gr systems especially when the shear strength of the metal/Gr interface is weak (e.g. Cu/Gr).

PH can be better understood by comparing our MD data to a simple model proposed in previous studies, which assume that the strength improvement from a periodic array of strong obstacles is dominated by the stress necessary to pull out the dislocation segments at the obstacles into a parallel dipole[45]

$$\Delta\sigma_{PH} = \frac{\mu b}{2\pi\lambda}\ln\left(\frac{b}{\lambda} + \frac{b}{D}\right)^{-1} \tag{2}$$

where μ is the shear modulus of Ni at 0.1 K (=76 GPa), b is the magnitude of the Burgers vector (=0.2496 nm) and $\lambda = L_x$

https://doi.org/10.1021/acsami.1c05129
ACS Appl. Mater. Interfaces XXXX, XXX, XXX−XXX

– D is the inter-obstacle spacing. In Figure 2e, we find good agreement between the strength improvements of IH obtained from our MD simulations and eq 2, further confirming that deformation is PH-dominated in the $D/L_x < 1$ regime. Having discussed the mechanism transition from IH to PH due to the loss of GDC integrity, we continue in the next section with considering the more realistic case of finite Grs and investigate the IH and PH mechanism as well as the associated transition, which has not been examined up to now.

3.2. PDL Pileup–Gr Interactions. In this section, we investigate the interactions between a PDL pileup and finite Grs via a novel nanoindentation configuration (Figure 1b). The obtained hardness–depth (H–d) curves of pure Ni and Ni/Gr composites are plotted in Figure 3a,b, respectively,

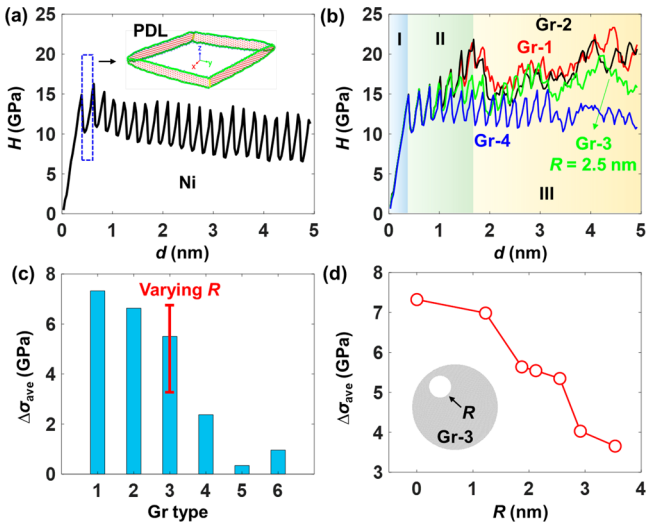

Figure 3. Simulation results of full 3D Ni and Ni/Gr samples with PDLs. (a) Hardness–depth (H–d) curves for pure Ni. (b) Hardness–depth (H–d) curves for Ni/Gr-1, Ni/Gr-2, Ni/Gr-3 (R = 2.5 nm), Ni/Gr-4. (c) Strength improvement for different types of Ni/Gr composites. (d) Strength improvement for Ni/Gr-3 with respect to the radius R of the void.

which feature different deformation stages. In Figure 3a, for Ni, periodic oscillations appear in the H–d curve; one period represents the formation and propagation of one PDL (Figure S5). In particular, the Ni/Gr composites have the same elastic response in stage I but different responses in other stages. For example, Gr-1 (defect-free Gr) and Gr-2 (Gr with a void in the center) exhibit a continuously increasing hardness in stage II and random fluctuations in stage III. By contrast, Gr-3 (Gr with a void at the PDL corner) and Gr-4 (the PDL is not fully within Gr) show a lower hardness in stages II and III. To gain a quantitative insight, the strength improvement $\Delta\sigma$ is defined as the average of the hardness difference between Ni/Gr and Ni in stages II and III and is plotted in Figure 3c, showing that the strength improvement of Ni/Gr composites depends on the GDC integrity. In order to demonstrate the complex coupling between void size, GDC integrity, Gr deformation, and localized dislocation evolution, we consider various void radii (R = 1.22, 1.87, 2.12, 2.55, 2.92, and 3.54 nm, which are denoted as Gr-3-1, ..., Gr-3-6) for Gr-3 (which was the only case for which the void radius R affected the deformation mechanism). In Figure 3d, it is seen that the strength improvement of Ni/Gr-3 decreases as the radius of the inner void increases.

The mechanical behavior of all samples can be understood by zooming in on their defect evolution with indentation. During the deformation of pure Ni, PDLs nucleate from the indenter, propagate downward, and leave from the free bottom repeatedly, leading to the periodic fluctuations in the H–d curve (Figure 3a) and permanent material flow without any plasticity being left in the sample (Figure S5f). The formation of PDLs has been studied in previous MD simulations, but it is relatively simple in the present simulation due to the carefully selected lattice orientations of the Ni matrix and the special indenter shape (see Figure S5a–e for the formation mechanism). It is worth noting that this is the first MD simulation that can produce the sequential PDLs in the same slip plane, providing a method to study the interactions between the PDL pileup and obstacles such as GBs, precipitates, and other interfaces in MD simulations.

To illustrate the deformation mechanisms of Ni/Gr-1, we present the nucleated dislocations at four critical points 1–4 during the simulations in Figure 4. At point 1, one PDL forms below the indenter (Figure 4b), leading to the first hardness drop in Figure 4a. The repeated formation and propagation of PDLs result in periodic hardness drops in stage II. At point 2, seven PDLs are produced, the first three of which are absorbed by the Ni/Gr interface (Figure 4c), and the remaining four form a pileup. The PDL pileup exerts a back stress to the indenter, resulting in the increasing hardening behavior in stage II. Similar to Figure 2b, the enlarged snapshots in Figure 4f show that the phase transition from FCC to HCP occurs at point 2 above Gr due to the dislocation absorption by core spreading, and Gr significantly deforms at locations where the interaction with PDLs takes place. Defect analysis shows that the phase transition from FCC to HCP occurs layer by layer near the Ni/Gr interface as more PDLs were absorbed by the interface, and the activation barrier for this phase transition can be simply quantified by the critical atomic von Mises stress (~30.0 GPa) at the transition front (Figure S6). The decrease of hardening after point 2 is because the Ni matrix itself cannot withstand the accumulated stress due to the PDL pileup, while Gr does not fracture or deform plastically. Since Gr can block all dislocations above it without dislocation bowing out or looping, it acts as an interface, resulting in the highest strengthening effect for the Ni/Gr composite. At point 3, the hardness significantly decreases due to the collapse of the PDL pileup (Figure 4d) by which two vertical stacking faults connect all PDLs. The atomistic mechanisms of this new collapse are provided in Figure S7. Meanwhile, more HCP Ni atoms are transformed above Gr, and Gr deforms more severely (Figure 4f). After point 3, new dislocations nucleate below the indenter, which interact with the existing dislocation network in the Ni matrix, resulting in the formation of a complex dislocation network instead of clear PDLs (Figure 4e). The HCP atoms above Gr disappear at point 4 because dislocation nucleation at the top Ni/Gr interface releases the accumulated stress. Note that no dislocations emerge below Gr, indicating that Gr has been a strong barrier to prevent dislocation transmission.

The reduced strengthening effect for Gr-3, Gr-4, Gr-5, and Gr-6 compared to Gr-1 and Gr-2 result from a different deformation mechanism. Here, we consider the results of Gr-4 as an example to illustrate the PDL pileup–Gr interaction mechanisms in Figure 5. A small window of fluctuations in the inset of Figure 5a is analyzed by visualizing the defective atoms and relative positions of C atoms in Gr along the z-direction in

https://doi.org/10.1021/acsami.1c05129
ACS Appl. Mater. Interfaces XXXX, XXX, XXX–XXX

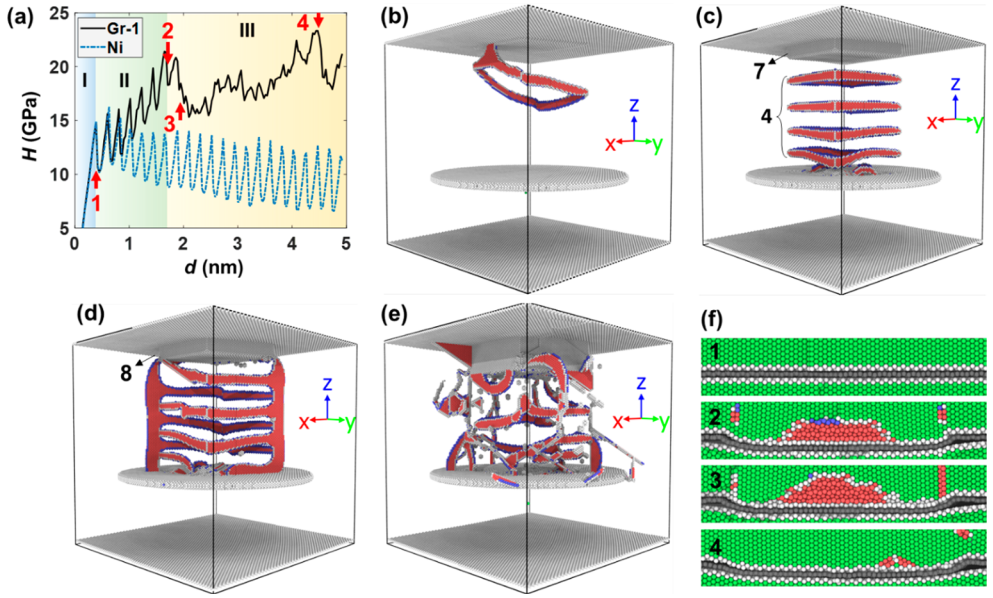

Figure 4. Simulation results of Ni/Gr-1. (a) Hardness−depth (H−d) curves. (b−e) Nucleated dislocations above Gr at points 1−4 in (a), respectively. (f) Phase transition at the Ni/Gr interface and deformed Gr at points 1−4 in (a), respectively. All FCC Ni atoms are removed by the CNA.

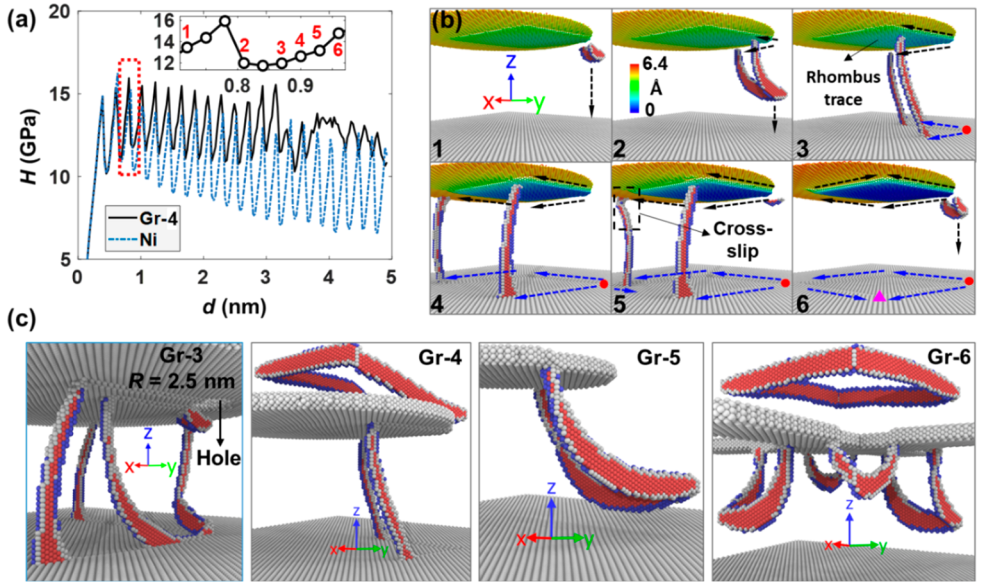

Figure 5. Simulation results of Ni/Gr-3, ..., Ni/Gr-6. (a) Hardness−depth curves of pure Ni and Ni/Gr-4. (b) Dislocation propagation by complex looping at points 1−6 in (a), respectively. C atoms are colored by their relative positions in the z-direction. (c) Dislocation propagation below Gr-3 (R = 2.5 nm), Gr-4, Gr-5, and Gr-6. All FCC Ni atoms in (b,c) are removed by the CNA.

Figure 5b. Six snapshots 1−6 correspond to the six points 1−6 in the inset of Figure 5a. Initially, the first PDL segments that are not within the Gr can move downward (Figure 5b1). Then, they bow out and continue to move and glide along the rhombus edges (deformation trace in Gr formed by the PDL−Gr interaction as shown by the green or blue C atoms in Figure 5b) as indicated by the black dashed arrows (Figure 5b2). When the second PDL approaches Gr-4, the dislocation segments continue to move to the free bottom. Consequently, two isolated ED pairs form, with one end being pinned to Gr and the other end being connected to the free bottom. These two dislocation pairs become screw dislocations, glide along the rhombus edges (Figure 5b3−6), and escape from the free bottom, leaving a rhombus atomic step at the bottom (Figure 5b6). Note that in this dislocation bypassing process, the dislocation cross-slip (Figure 5b5) caused by the high local stress plays a crucial role in changing the slip directions such that the screw dislocations below Gr can glide along the deformed rhombus trace (Figure S8). The relative positions of C atoms in Figure 5b indicate that Gr is gradually sheared in the regions where the dislocations glide below it. Similarly, Figure 5c presents the key snapshots of dislocation−Gr interactions of Gr-3, Gr-4, Gr-5, and Gr-6. All the dislocation segments that are not within Gr are able to continue to propagate by a similar dislocation bow-out and looping mechanism. Therefore, this deformation mechanism can be considered a complex Orowan looping mechanism by

https://doi.org/10.1021/acsami.1c05129
ACS Appl. Mater. Interfaces XXXX, XXX, XXX−XXX

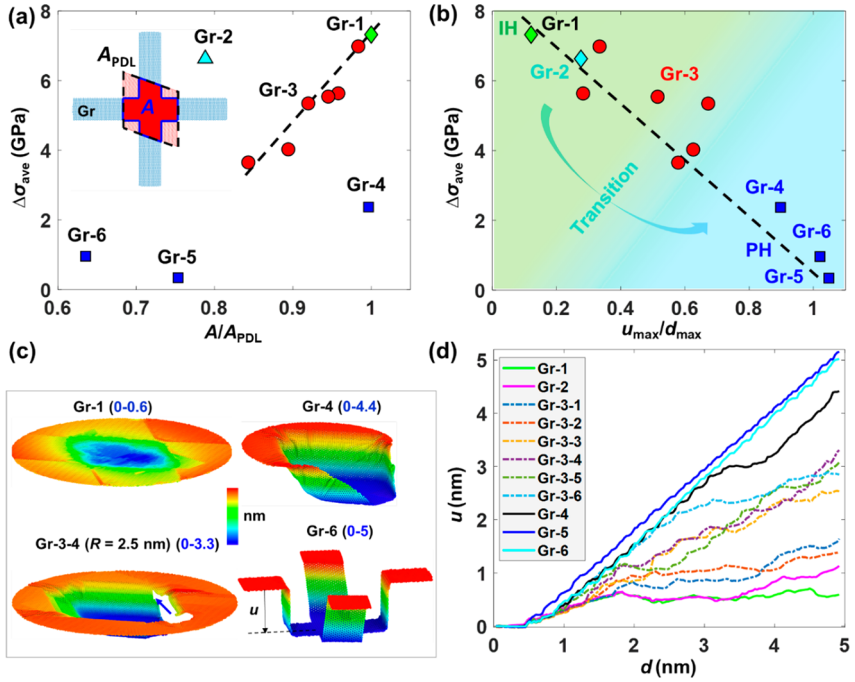

Figure 6. Overall IH-to-PH transition. (a) Dependence of the average strength improvement ($\Delta\sigma_{ave}$) with respect to the area ratio A/A_{PDL}. (b) Dependence of the average strength improvement ($\Delta\sigma_{ave}$) with respect to the dimensionless maximum deflection of Grs (u_{max}/d_{max}). (c) Deformed Grs at the end of deformation. C atoms are colored by the relative positions in the z-direction. (d) Evolution of out-of-plane deformation (u) of Grs.

dislocation cross-slip such that the strength improvement of these Ni/Gr composites results from PH.

The above simulation results suggest two strengthening mechanisms in PDL pileup−Gr interactions: IH (Figure 4) and PH (Figure 5). In IH, an efficient strengthening effect is realized as PDLs pile up at Gr without being able to transmit across it. In PH, the strengthening effect is less significant, and dislocations bow out and loop to bypass Gr gradually. From the perspective of Gr deformation, the whole Gr needs to be sheared simultaneously once dislocation transmission takes place during IH (Figure 4), whereas Gr is gradually and locally sheared as dislocations glide along the deformed rhombus trace as seen in PH (Figure 5). This change in Gr deformation and interaction with dislocations during deformation give rise to the different strengthening effect (Figure 3c). Based on Figures 4 and 5, it is seen that IH and PH are reminiscent of the classical model of dislocation movement in crystals: (i) IH is like the breaking of all the bonds on an entire plane of atoms at once and (ii) PH is like the breaking and reforming of a line of bonds one (or a few) at a time;[46] the latter is much easier than the former.

3.3. IH-to-PH Transition. The results in Figures 3c,d and 4, 5 also suggest that IH and PH are not fully isolated; most cases examined here instead undergo a transition between IH and PH. For example, the strengthening effect of Gr-3 "ranges" from pure IH (such as Gr-1 and Gr-2) and pure PH (such as Gr-4, Gr-5, and Gr-6), heavily depending on the void sizes on Gr-3 (as well as on the deformation level as discussed later on). These observations raise the natural question of what indicates or controls the strengthening role of Gr in a metal matrix. Here, we propose that GDC integrity, Gr deformation, and dislocation evolution in the Ni matrix collaboratively affect the strengthening effect of a Gr inclusion.

Geometrically, when the incoming dislocations are fully within Gr, the GDC integrity is the highest and therefore Gr is more likely to act as an interface to block dislocation motion (Figures 2b and 4). The Gr with good GDC integrity could be without interior voids (Gr-1) or defective as long as the internal voids are not on the propagation path of dislocations (Gr-2). The GDC integrity is reduced once Gr cannot block all incoming dislocations (free Gr in Figure 2d and Gr-3, Gr-4, Gr-5, and Gr-6 in Figure 5). To quantitatively illustrate the influence of GDC integrity on the strengthening mechanism, we first introduce a geometrical parameter A/A_{PDL}, where A_{PDL} denotes the area of the PDL and A denotes the area of Gr within the PDL (see inset in Figure 6a). In Figure 6a the average strength improvement $\Delta\sigma_{ave}$ of all Ni/Gr composites is plotted with respect to this parameter A/A_{PDL}. The strength improvement is found to be related to A/A_{PDL} for Gr-1 and Gr-3 with varying R but not for Gr-2, Gr-4, Gr-5, and Gr-6. This implies that the strengthening effect is not simply determined by the geometry of the inserted Grs.

In order to relate the strength improvement of Ni/Gr composites to Gr deformation, we define the ratio u_{max}/d_{max}, where u_{max} denotes the maximum out-of-plane deflection of Gr along the z-direction as shown in Figure 6c and d_{max} denotes the maximum applied indentation magnitude. u_{max}/d_{max} therefore represents how much Gr is deformed under the external loading from the indenter. In Figure 6b, we show that $\Delta\sigma_{ave}$ is inversely proportional to u_{max}/d_{max} for all Grs considered. A smaller value for u_{max}/d_{max} indicates that Gr cannot be deformed much and results in a good strengthening effect. We also indicate the type of strengthening mechanisms: Ni/Gr-1 and Ni/Gr-2 are IH-dominated and Ni/Gr-4, Ni/Gr-5, and Ni/Gr-6 are PH-dominated, while for Ni/Gr-3 transitions occur between IH and PH as R varies. Therefore, IH corresponds to small u_{max}/d_{max} and a high strengthening

https://doi.org/10.1021/acsami.1c05129
ACS Appl. Mater. Interfaces XXXX, XXX, XXX−XXX

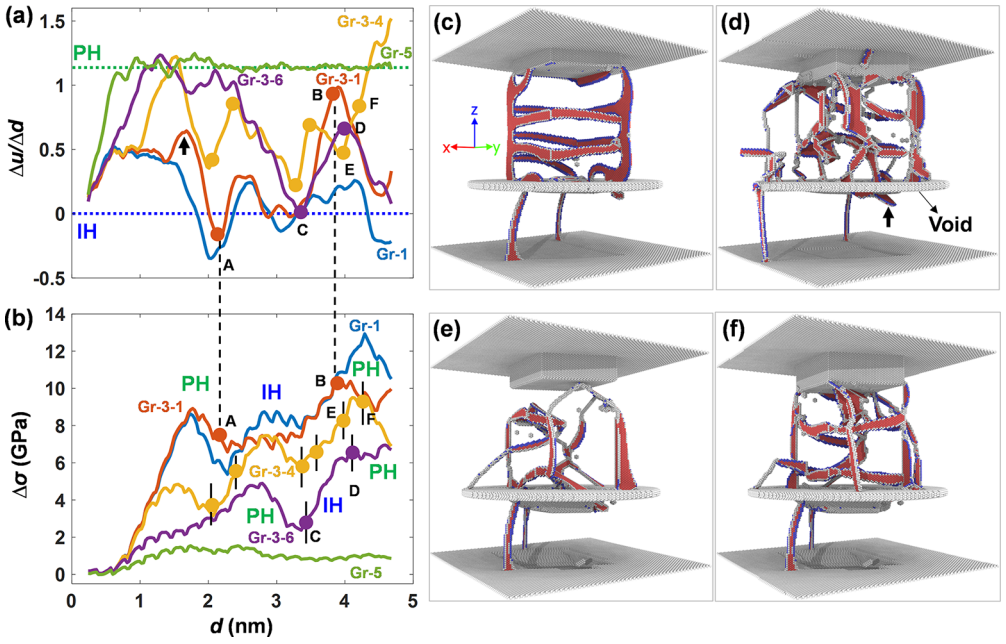

Figure 7. Local IH-to-PH transition. (a) Evolution of deformation rate ($\Delta u/\Delta d$) for Gr-1, Gr-3-1, Gr-3-4, Gr-3-6, and Gr-5. (b) Evolution of the strengthening effect. (c–f) Nucleated dislocations in the systems at points A–D in (a,b), respectively. All FCC Ni atoms in (c–f) are removed by the CNA.

effect ($\Delta\sigma_{ave}$), whereas PH corresponds to large u_{max}/d_{max} and a low strengthening effect ($\Delta\sigma_{ave}$). This relationship can be further understood by the deformation of Grs at the end of the simulations as shown in Figure 6c. Our previous MD simulations for Cu/Gr systems have shown that out-of-plane deflection of Gr (u) was caused by dislocation transmission.[34] A larger u_{max} indicates less dislocation storage near Gr and lower strengthening and vice versa.

Although u_{max} is an excellent indicator of the average strengthening effect up to an indentation depth of d_{max}, we show that such an overall observation can "ignore" the underlying mechanisms and the specific strengthening effect could vary between IH and PH even for the same Gr under different indentation depths. Therefore, we look at the local response at different depths. Our MD simulations allow to capture each incremental step during the sequential PDLs, showing the detailed microstructural evolution. The out-of-plane deformation (u) evolution of all Grs is plotted as a function of the indentation depth in Figure 6d. We find that in general, Gr deformation (u) increases with increasing indentation depth (d) but the u–d slopes are far from constant.

This observation motivates the analysis of the evolution of the deformation rate $\Delta u/\Delta d$ of Grs and the corresponding strength improvement at each loading step (Figure 7a,b), where $\Delta u/\Delta d$ is obtained by calculating the local slope of the curves in Figure 6c and therefore represents the real-time deformation of Grs. Two natural limiting cases are: (i) $\Delta u/\Delta d \sim 1$ means that the applied displacement Δd from the indenter instantly causes the same amount of out-of-plane deformation Δu in Grs (i.e., Grs barely contribute to the strengthening). This limit may represent a pure PH mechanism, as represented by Gr-5 and Gr-6. (ii) $\Delta u/\Delta d \sim 0$ means that all the deformation from the indenter was blocked by Grs. This limit may represent a pure IH mechanism, as represented by Gr-1 and Gr-2. Note that at the end of deformation, IH-to-PH occurred in Ni/Gr-2 as shown in Figure S9, leading to a slightly lower stress than Ni/Gr-1 in Figures 3 and 6.

We conclude by focusing on Gr-3 with three different void sizes (R values) (Figure 7a,b): Gr-3-1 with R = 1.2 nm, Gr-3-4 with R = 2.5 nm, and Gr-3-6 with R = 3.5 nm. In this case, IH and PH take effect locally and sequentially, manifesting as an overall mixed state between IH and PH. In particular, Gr-3-1 acts as a precipitate before point A as evidenced by a peak in $\Delta u/\Delta d$ (see arrow in Figure 7a) and two dislocation segments bypass below Gr (see Figure 7c). From point A to B, $\Delta u/\Delta d \sim 0$ and $\Delta\sigma$ increases continuously, indicating that Gr-3-1 in this regime acts as an interface to strengthen the Ni matrix. This can be further evidenced in Figure 7d as no new dislocations bypass Gr from A to B even though the dislocation density increases from 2.64×10^{14} m^{-2} (Figure 7c) to 3.88×10^{14} m^{-2} (Figure 7d) above Gr. At point B, a new dislocation with a different slip system nucleates below the Gr as indicated by the arrow in Figure 7d. The reason for the transition from PH to IH may be the fact that PDLs start interacting with each other (Figure 6c). This results in the collapse of the PDL pileup (similar to Figure 4d), which could change the slip direction of dislocations such that they do not encounter the void, and therefore Gr blocks their movement. This behavior is similar to the cases of highest GDC integrity (such as Gr-1 and Gr-2). Therefore, PH-to-IH transition occurs due to the evolved GDC during deformation. Afterward, when the accumulated stress activates the dislocation motion near the void as indicated by the arrow in Figure 7d, the ratio of $\Delta u/\Delta d$ increases and $\Delta\sigma$ decreases. As a result, Gr acts as a precipitate again, and dislocations continue to propagate by bow-out and Orowan looping. Similar PH-IH-PH transitions are also observed for Gr-3-4: IH dominates between points C and D, corresponding to the nucleated dislocations in Figure 7e,f with the dislocation density increasing from 2.22×10^{14} to 2.75×10^{14} m^{-2}. For Gr-3-4, multiple transitions are captured as indicted by the yellow points in Figure 7a,b.

https://doi.org/10.1021/acsami.1c05129
ACS Appl. Mater. Interfaces XXXX, XXX, XXX–XXX

Another interesting observation is that a crack initiated from the edge of the inner void and propagated along the PDL edge in Gr-3-4 at point F (Figures 6c and S10), leading to the abrupt increase of $\Delta u/\Delta d$ and the dramatic reduction of $\Delta\sigma$. Once Gr fractures, it loses its ability to act as an interface and results in PH thereafter without being able to transition back to IH. Even though Gr is much stronger than Ni, the local defects near the void can induce a high stress concentration due to the PDL pileup. In Figure S10, it is seen that cracks initiated once the local stress near the void exceeded the strength of Gr. Interestingly, in Figure S11, we also see that the fracture behavior of Gr in Ni/Gr-3 depends on the radius (R) of the void within the Gr. The Grs with a small void ($R \leq 1.8$ nm) and a large void ($R > 3.5$ nm) did not fracture, while the Grs with a medium-sized void ($R = 2.1$, 2.5 and 2.9 nm) fractured. This finding can be used to guide the design of stronger metal/Gr composites if void-like defects in Gr are inevitable.

Even though our simulations mainly focus on Gr with ideal geometries, our findings imply the following: first, instead of being isolated, the two well-recognized strengthening mechanisms, that is, IH and PH, are somewhat transitional as the dislocations interact with local structures, which is new to our knowledge. In addition to Gr, the transition may occur in other obstacle strengthening processes, such as nano-precipitates in alloy metals, as long as the integrity of the obstacle-dislocation configuration is changed during deformation. Second, for a given obstacle (Gr), its strengthening role will not always be the same since the size, position, and type of incoming dislocations keep evolving. For example, experiments have shown that continuous indentation resulted in an increase of PDL size,[47] and our simulations imply that the initial PDL−obstacle interactions could be IH-dominated and the latter PDL−obstacle interactions could be PH-dominated once the nucleated PDLs are not fully within the obstacles. Third, the present simulations demonstrate that a large and complete Gr should be used in efforts to enhance the strength of the metal matrix. The dual role comes from the fact that large Gr mainly acts as an interface to block dislocations with a strong strengthening effect, whereas a smaller-sized Gr with defects acts as a source to nucleate dislocations and a precipitate to impede dislocations with a weak strengthening effect. This may explain the huge difference in the strengthening effect between metal/Gr nanolayered composites and metal/Gr composites with randomly dispersed Gr.[15,48] Lastly, our results demonstrate a close relationship between the dislocation−graphene interaction and real-time deformation $\Delta u/\Delta d$ in Gr. This relation may provide an effective method for determining the detailed strengthening effect in a metal/Gr composite simply by examining the strain transferred from the external load to the embedded Gr sheet. Although this methodology has been used to study the stress transfer problem in Gr/polymer systems,[49−51] it has not been used to assess the performance of metal/Gr composites.

4. CONCLUSIONS

In summary, this article presents, for the first time, systematic MD simulations and an in-depth analysis to study the dislocation-Gr interactions and the transition from IH to PH in Ni/Gr composites, providing a better understanding of known IH and PH and connections between them. Second, graphene's deformability is found to be an effective signature to indicate the real-time strengthening degree, revealing that the integrity of the GDC, graphene deformation and dislocation evolution in the Ni matrix collaboratively determine the strengthening effect. Finally, our analysis suggests that a large-size and defect-free Gr is preferred to achieve a better strengthening effect.

■ ASSOCIATED CONTENT

Supporting Information

The Supporting Information is available free of charge at https://pubs.acs.org/doi/10.1021/acsami.1c05129.

Ni/Gr interface sliding when a dislocation bypasses graphene; formation and propagation of a PDL in Ni; PDL pileup collapse mechanisms; dislocation cross-slip when a PDL bypasses Gr; simulation results of Ni/Gr-2; simulation results of Ni/Gr-3 ($R = 2.5$ nm); Gr fracture behaviors in Ni/Gr-3; effects of boundary conditions and temperature; phase transformation at the Ni/Gr interface; and dislocation core spreading (PDF)

ED−Gr interactions with IH (MOV)

ED−Gr interactions with PH (MOV)

PDL−Gr interactions using Gr-1 (MOV)

PDL−Gr interactions using Gr-3 (MOV)

PDL−Gr interactions using Gr-4 (MOV)

PDL−Gr interactions using Gr-5 (MOV)

PDL−Gr interactions using Gr-6 (MOV)

■ AUTHOR INFORMATION

Corresponding Author

Katerina E. Aifantis − *Department of Mechanical and Aerospace Engineering, University of Florida, Gainesville, Florida 32611, United States;* orcid.org/0000-0002-0105-548X; Phone: 352 392-6227; Email: kaifantis@ufl.edu

Authors

Fei Shuang − *Department of Mechanical and Aerospace Engineering, University of Florida, Gainesville, Florida 32611, United States*

Zhaohe Dai − *Mathematical Institute, University of Oxford, Oxford OX2 6GG, U.K.*

Complete contact information is available at: https://pubs.acs.org/10.1021/acsami.1c05129

Author Contributions

K.E.A and F.S. conceived the research. F.S. carried out the MD simulations. F.S., Z.D. and K.E.A analyzed the results and wrote the paper. All authors reviewed and approved the manuscript.

Notes

The authors declare no competing financial interest.

All data required to reproduce the findings during this study are included in this article and the Supporting Information.

■ ACKNOWLEDGMENTS

Authors K.E.A. and F.S. are grateful for the support of the U.S. Department of Energy, Office of Basic Energy Sciences under grant DE-SC0017715, which made this work possible. Author Z.D. acknowledges funding from the European Union's Horizon 2020 research and innovation programme under the Marie Skłodowska-Curie grant agreement no. 886028.

REFERENCES

(1) Bacon, D. J.; Osetsky, Y. N.; Rodney, D. Chapter 88 Dislocation-Obstacle Interactions at the Atomic Level. *Dislocations in Solids*; Elsevier, 2009; pp 1−90.

(2) Shuang, F.; Aifantis, K. E. Using Molecular Dynamics to Determine Mechanical Grain Boundary Energies and Capture Their Dependence on Residual Burgers Vector, Segregation and Grain Size. *Acta Mater.* **2020**, *195*, 358−370.

(3) Wei, Y.; Li, Y.; Zhu, L.; Liu, Y.; Lei, X.; Wang, G.; Wu, Y.; Mi, Z.; Liu, J.; Wang, H.; Gao, H. Evading the Strength-Ductility Trade-off Dilemma in Steel through Gradient Hierarchical Nanotwins. *Nat. Commun.* **2014**, *5*, 3580.

(4) Cheng, Z.; Zhou, H.; Lu, Q.; Gao, H.; Lu, L. Extra Strengthening and Work Hardening in Gradient Nanotwinned Metals. *Science* **2018**, *362*, No. eaau1925.

(5) Wang, Y.; Li, J.; Hamza, A. V.; Barbee, T. W. Ductile Crystalline-Amorphous Nanolaminates. *Proc. Natl. Acad. Sci.* **2007**, *104*, 11155−11160.

(6) Aifantis, K. E.; Willis, J. R. The Role of Interfaces in Enhancing the Yield Strength of Composites and Polycrystals. *J. Mech. Phys. Solid.* **2005**, *53*, 1047−1070.

(7) Soer, W. A.; Aifantis, K. E.; De Hosson, J. T. M. Incipient Plasticity during Nanoindentation at Grain Boundaries in Body-Centered Cubic Metals. *Acta Mater.* **2005**, *53*, 4665−4676.

(8) Malow, T. R.; Koch, C. C. Mechanical Properties in Tension of Mechanically Attrited Nanocrystalline Iron by the Use of the Miniaturized Disk Bend Test. *Acta Mater.* **1998**, *46*, 6459−6473.

(9) Conrad, H. Grain-Size Dependence of the Flow Stress of Cu from Millimeters to Nanometers. *Metall. Mater. Trans. A* **2004**, *35*, 2681−2695.

(10) Lu, L.; Chen, X.; Huang, X.; Lu, K. Revealing the Maximum Strength in Nanotwinned Copper. *Science* **2009**, *323*, 607−610.

(11) Li, X.; Wei, Y.; Lu, L.; Lu, K.; Gao, H. Dislocation Nucleation Governed Softening and Maximum Strength in Nano-Twinned Metals. *Nature* **2010**, *464*, 877−880.

(12) Tian, Y.; Xu, B.; Yu, D.; Ma, Y.; Wang, Y.; Jiang, Y.; Hu, W.; Tang, C.; Gao, Y.; Luo, K.; Zhao, Z.; Wang, L.-M.; Wen, B.; He, J.; Liu, Z. Ultrahard Nanotwinned Cubic Boron Nitride. *Nature* **2013**, *493*, 385−388.

(13) Huang, Q.; Yu, D.; Xu, B.; Hu, W.; Ma, Y.; Wang, Y.; Zhao, Z.; Wen, B.; He, J.; Liu, Z.; Tian, Y. Nanotwinned Diamond with Unprecedented Hardness and Stability. *Nature* **2014**, *510*, 250−253.

(14) Wang, J.; Zhou, Q.; Shao, S.; Misra, A. Strength and Plasticity of Nanolaminated Materials. *Mater. Res. Lett.* **2017**, *5*, 1−19.

(15) Kim, Y.; Lee, J.; Yeom, M. S.; Shin, J. W.; Kim, H.; Cui, Y.; Kysar, J. W.; Hone, J.; Jung, Y.; Jeon, S.; Han, S. M. Strengthening Effect of Single-Atomic-Layer Graphene in Metal-Graphene Nanolayered Composites. *Nat. Commun.* **2013**, *4*, 2114.

(16) Kim, S.-H.; Kim, H.; Kim, N. J. Brittle Intermetallic Compound Makes Ultrastrong Low-Density Steel with Large Ductility. *Nature* **2015**, *518*, 77−79.

(17) Jiang, S.; Wang, H.; Wu, Y.; Liu, X.; Chen, H.; Yao, M.; Gault, B.; Ponge, D.; Raabe, D.; Hirata, A.; Chen, M.; Wang, Y.; Lu, Z. Ultrastrong Steel via Minimal Lattice Misfit and High-Density Nanoprecipitation. *Nature* **2017**, *544*, 460−464.

(18) He, J. Y.; Wang, H.; Huang, H. L.; Xu, X. D.; Chen, M. W.; Wu, Y.; Liu, X. J.; Nieh, T. G.; An, K.; Lu, Z. P. A Precipitation-Hardened High-Entropy Alloy with Outstanding Tensile Properties. *Acta Mater.* **2016**, *102*, 187−196.

(19) Ming, K.; Bi, X.; Wang, J. Realizing Strength-Ductility Combination of Coarse-Grained $Al_{0.2}Co_{1.5}CrFeNi_{1.5}Ti_03$ Alloy via Nano-Sized, Coherent Precipitates. *Int. J. Plast.* **2018**, *100*, 177−191.

(20) Fu, Z.; Jiang, L.; Wardini, J. L.; MacDonald, B. E.; Wen, H.; Xiong, W.; Zhang, D.; Zhou, Y.; Rupert, T. J.; Chen, W.; Lavernia, E. J. A High-Entropy Alloy with Hierarchical Nanoprecipitates and Ultrahigh Strength. *Sci. Adv.* **2018**, *4*, No. eaat8712.

(21) Peng, S.; Wei, Y.; Gao, H. Nanoscale Precipitates as Sustainable Dislocation Sources for Enhanced Ductility and High Strength. *Proc. Natl. Acad. Sci.* **2020**, *117*, 5204−5209.

(22) Hwang, J.; Yoon, T.; Jin, S. H.; Lee, J.; Kim, T.-S.; Hong, S. H.; Jeon, S. Enhanced Mechanical Properties of Graphene/Copper Nanocomposites Using a Molecular-Level Mixing Process. *Adv. Mater.* **2013**, *25*, 6724−6729.

(23) Hwang, B.; Kim, W.; Kim, J.; Lee, S.; Lim, S.; Kim, S.; Oh, S. H.; Ryu, S.; Han, S. M. Role of Graphene in Reducing Fatigue Damage in Cu/Gr Nanolayered Composite. *Nano Lett.* **2017**, *17*, 4740−4745.

(24) Yang, Z.; Wang, D.; Lu, Z.; Hu, W. Atomistic Simulation on the Plastic Deformation and Fracture of Bio-Inspired Graphene/Ni Nanocomposites. *Appl. Phys. Lett.* **2016**, *109*, 191909.

(25) Shuang, F.; Aifantis, K. E. Relating the Strength of Graphene/Metal Composites to the Graphene Orientation and Position. *Scr. Mater.* **2020**, *181*, 70−75.

(26) Liu, X.; Wang, F.; Wang, W.; Wu, H. Interfacial Strengthening and Self-Healing Effect in Graphene-Copper Nanolayered Composites under Shear Deformation. *Carbon* **2016**, *107*, 680−688.

(27) Vardanyan, V. H.; Urbassek, H. M. Dislocation Interactions during Nanoindentation of Nickel-Graphene Nanocomposites. *Comput. Mater. Sci.* **2019**, *170*, 109158.

(28) Liu, X.; Wang, F.; Wu, H.; Wang, W. Strengthening Metal Nanolaminates under Shock Compression through Dual Effect of Strong and Weak Graphene Interface. *Appl. Phys. Lett.* **2014**, *104*, 231901.

(29) He, Z.; Zhu, Y.; Xia, J.; Wu, H. Optimization Design on Simultaneously Strengthening and Toughening Graphene-Based Nacre-like Materials through Noncovalent Interaction. *J. Mech. Phys. Solid.* **2019**, *133*, 103706.

(30) Wang, L.; Jin, J.; Yang, P.; Li, S.; Tang, S.; Zong, Y.; Peng, Q. Effect of Interfacial Bonding on Dislocation Strengthening in Graphene Nanosheet Reinforced Iron Composite: A Molecular Dynamics Study. *Comput. Mater. Sci.* **2021**, *191*, 110309.

(31) Zhu, J.; Liu, X.; Zhou, X.; Yang, Q. Strengthening Effect of Graphene-Edge Dislocation Interaction in Graphene Reinforced Copper Matrix Composites. *Comput. Mater. Sci.* **2021**, *188*, 110179.

(32) Plimpton, S. Fast Parallel Algorithms for Short-Range Molecular Dynamics. *J. Comput. Phys.* **1995**, *117*, 1−19.

(33) Xiao, P.; Wang, J.; Yang, R.; Ke, F.; Bai, Y. Transition of Mechanisms Underlying the Rate Effects and Its Significance. *Comput. Mater. Sci.* **2015**, *98*, 70−75.

(34) Shuang, F.; Aifantis, K. E. Dislocation-Graphene Interactions in Cu/Graphene Composites and the Effect of Boundary Conditions: A Molecular Dynamics Study. *Carbon* **2021**, *172*, 50−70.

(35) Mendelev, M. I.; Kramer, M. J.; Hao, S. G.; Ho, K. M.; Wang, C. Z. Development of Interatomic Potentials Appropriate for Simulation of Liquid and Glass Properties of $NiZr_2$ Alloy. *Philos. Mag.* **2012**, *92*, 4454−4469.

(36) Hossain, M. Z.; Hao, T.; Silverman, B. Stillinger-Weber Potential for Elastic and Fracture Properties in Graphene and Carbon Nanotubes. *J. Phys. Condens. Matter* **2018**, *30*, 055901.

(37) Santhapuram, R. R.; Muller, S. E.; Nair, A. K. Nanoscale Bending Properties of Bio-Inspired Ni-Graphene Nanocomposites. *Compos. Struct.* **2019**, *220*, 798−808.

(38) Stukowski, A. Visualization and Analysis of Atomistic Simulation Data with OVITO-the Open Visualization Tool. *Modell. Simul. Mater. Sci. Eng.* **2010**, *18*, 015012.

(39) Stukowski, A. Structure Identification Methods for Atomistic Simulations of Crystalline Materials. *Modell. Simul. Mater. Sci. Eng.* **2012**, *20*, 045021.

(40) Stukowski, A.; Bulatov, V. V.; Arsenlis, A. Automated Identification and Indexing of Dislocations in Crystal Interfaces. *Modell. Simul. Mater. Sci. Eng.* **2012**, *20*, 085007.

(41) Ardell, A. J. Precipitation Hardening. *Metall. Trans. A* **1985**, *16*, 2131−2165.

(42) Hall, E. O. The Deformation and Ageing of Mild Steel: III Discussion of Results. *Proc. Phys. Soc., London, Sect. B* **1951**, *64*, 747−753.

(43) Petch, N. J. The Cleavage Strength of Polycrystals. *J. Iron Steel Inst.* **1953**, *174*, 25−28.

https://doi.org/10.1021/acsami.1c05129
ACS Appl. Mater. Interfaces XXXX, XXX, XXX−XXX

(44) Shaw, L. L.; Ortiz, A. L.; Villegas, J. C. Hall-Petch Relationship in a Nanotwinned Nickel Alloy. *Scr. Mater.* **2008**, *58*, 951−954.
(45) Bacon, D. J.; Kocks, U. F.; Scattergood, R. O. The Effect of Dislocation Self-Interaction on the Orowan Stress. *Philos. Mag.* **1973**, *28*, 1241−1263.
(46) Taylor, G. I. The Mechanism of Plastic Deformation of Crystals. Part I.—Theoretical. *Proc. R. Soc. Lond. -Ser. A Contain. Pap. a Math. Phys. Character* **1934**, *145*, 362−387.
(47) Lee, S.; Vaid, A.; Im, J.; Kim, B.; Prakash, A.; Guénolé, J.; Kiener, D.; Bitzek, E.; Oh, S. H. In-Situ Observation of the Initiation of Plasticity by Nucleation of Prismatic Dislocation Loops. *Nat. Commun.* **2020**, *11*, 2367.
(48) Yazdandoost, F.; Yari Boroujeni, A.; Mirzaeifar, R. Nanocrystalline Nickel-Graphene Nanoplatelets Composite: Superior Mechanical Properties and Mechanics of Properties Enhancement at the Atomistic Level. *Phys. Rev. Mater.* **2017**, *1*, 076001.
(49) Papageorgiou, D. G.; Kinloch, I. A.; Young, R. J. Mechanical Properties of Graphene and Graphene-Based Nanocomposites. *Prog. Mater. Sci.* **2017**, *90*, 75−127.
(50) Dai, Z.; Liu, L.; Zhang, Z. Strain Engineering of 2D Materials: Issues and Opportunities at the Interface. *Adv. Mater.* **2019**, *31*, 1805417.
(51) Dai, Z.; Lu, N.; Liechti, K. M.; Huang, R. Mechanics at the Interfaces of 2D Materials: Challenges and Opportunities. *Curr. Opin. Solid State Mater. Sci.* **2020**, *24*, 100837.

https://doi.org/10.1021/acsami.1c05129
ACS Appl. Mater. Interfaces XXXX, XXX, XXX−XXX